Chapter 45
Characterization of Active Microcantilevers Using Laser Doppler Vibrometry

Michael G. Ruppert, Natã F. S. De Bem, Andrew J. Fleming, and Yuen K. Yong

45.1 Introduction

The microcantilever is a microelectromechanical systems (MEMS) device and is a key enabling technology for scanning probe microscopes, scanning probe lithography systems, and probe-based data storage systems [1]. One of the most celebrated uses of the microcantilever is for atomic force microscopy (AFM) [2]. Due to its unprecedented resolution, AFM has driven major breakthroughs in material science, surface science, and bio-nanotechnology.

In dynamic AFM, the cantilever is actively driven at one of its resonance frequencies, while a sample is scanned underneath a sharp tip. By controlling changes in the oscillation amplitude of the cantilever using a feedback control loop, a 3D image of the surface as well as of nanomechanical sample properties can be obtained [1]. Most conventional AFM systems employ piezoacoustic base-excitation and an optical beam deflection sensor to induce and measure the corresponding vibrations. However, this excitation scheme yields distorted frequency responses (compare Fig. 45.3d) and the optical measurement can require tedious laser alignment and relies on a sufficiently large cantilever with a reflective surface for optimal transduction [3]. As a result, substantial research efforts have gone into active cantilevers with integrating actuation and sensing on the cantilever chip level [4–6].

In this work, we investigate three different cantilever geometries with integrated piezoelectric actuation and sensing which are shown in Fig. 45.1. Each cantilever consists of a device layer of single-crystal silicon with a thickness of 10 μm, one or two 0.5 μm thick regions of piezoelectric aluminum-nitrate (AlN) for actuation and

M. G. Ruppert (✉) · N. F. S. De Bem · A. J. Fleming · Y. K. Yong
The University of Newcastle, Callaghan, NSW, Australia
e-mail: michael.ruppert@newcastle.edu.au; n.francosoaresdebem@uon.edu.au; andrew.fleming@newcastle.edu.au; yuenkuan.yong@newcastle.edu.au

© Springer Nature Switzerland AG 2021

S. Oberst et al. (eds.), *Vibration Engineering for a Sustainable Future*,
https://doi.org/10.1007/978-3-030-48153-7_45

Fig. 45.1 Design layout of the three cantilever designs investigated in this work with (**a**) rectangular, (**b**) triangular, and (**c**) stepped rectangular geometry

sensing and a 1µm layer of aluminum for electrical connections. The top surface of the device layer is n-doped and serves as the ground return for the piezoelectric transducers. With this layout, the devices can be fabricated with the rapid MEMS prototyping process PiezoMUMPS® (MEMSCAP Inc.).

45.2 Dynamic Analyses Using Laser Doppler Vibrometry

In this section, the analysis and characterization of the deflection mode-shapes, system identification including actuator and sensor calibration, and the calibration of the dynamic parameters of the cantilever eigenmodes is performed with laser Doppler vibrometry (LDV) using a Polytec MSA-100-3D. LDV has demonstrated significant influence in the field of experimental structural analysis of MEMS [7].

45.2.1 Modal Analysis

In order to experimentally obtain the mode shapes using LDV, the piezoelectric layers are excited with a low-voltage periodic chirp signal, while the cantilevers are scanned underneath the laser. Depending on the geometry of the cantilever, an appropriate scan point layout is chosen with 150–300 scan points as shown in Fig. 45.2. For each scan point, the frequency response from actuation voltage to deflection is obtained by taking the FFT of the velocity and reference signal with 25 complex averages and performing the integration in the frequency domain. When the magnitude spectrum is plotted against the scan point location, the deflection mode shapes as shown in Fig. 45.2 are obtained. It can be noticed that while the first three flexural modes of the rectangular cantilever follow the theoretical Euler Bernoulli mode shapes, the third modes of the triangular and stepped rectangular show deviations. Due to the large base of the stepped rectangular cantilever, it's third mode follows the mode shape predicted by Mindlin plate theory [8].

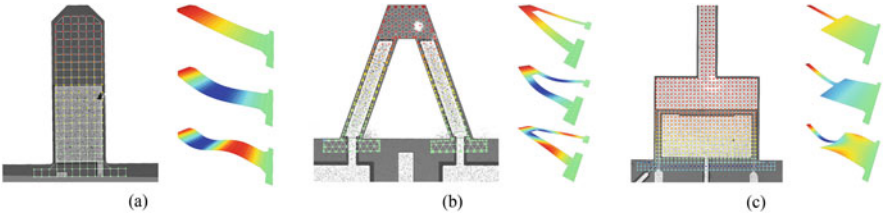

Fig. 45.2 Modal analysis of the first three flexural eigenmodes of three different cantilever geometries using a laser Doppler vibrometer

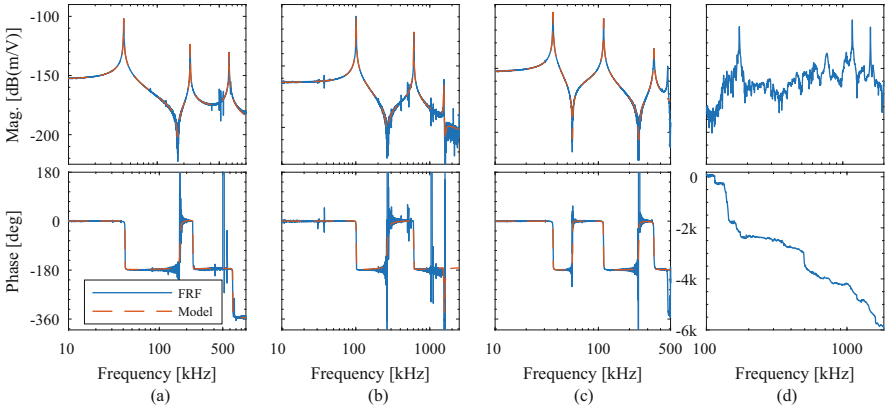

Fig. 45.3 Frequency response function (FRF) and identified model of the cantilevers. (**a**) Rectangular. (**b**) Triangular. (**c**) Stepped. (**d**) Stack-actuated

45.2.2 System Identification

The frequency response from piezoelectric actuation voltage to the tip deflection is obtained by considering only one scan point near the tip. The measured responses up to the third flexural mode as well as the identified models are shown in Fig. 45.3a–c. The identified models are of the form [9]

$$G_{\text{vib}}(s) = \sum_{i=1}^{3} \frac{\alpha_i \omega_i^2}{s^2 + \frac{\omega_i}{Q_i} s + \omega_i^2} + D, \tag{45.1}$$

where α_i, ω_i, Q_i are the actuation gain, natural resonance frequency, and quality factor of the i-th mode. If two consecutive α_i are of opposing sign, a non-collocated system is obtained (Fig. 45.3a and b); otherwise the system is said to be collocated (Fig. 45.3c) [10]. As the magnitude responses are in units of dB(m/V), the actuation gains at each resonance can be extracted directly (compare Table 45.1). Note that the response shown in Fig. 45.3d obtained from a conventional piezoacoustic base-

Table 45.1 Cantilever parameters obtained from (**a**) experiment and (**b**) FEA

	Rectangular				Triangular				Stepped			
Mode	f_i [kHz]	Q_i	k_i $\left[\frac{\mathrm{N}}{\mathrm{m}}\right]$	α_i $\left[\frac{\mathrm{nm}}{\mathrm{mV}}\right]$	f_i [kHz]	Q_i	k_i $\left[\frac{\mathrm{N}}{\mathrm{m}}\right]$	α_i $\left[\frac{\mathrm{nm}}{\mathrm{mV}}\right]$	f_i [kHz]	Q_i	k_i $\left[\frac{\mathrm{N}}{\mathrm{m}}\right]$	α_i $\left[\frac{\mathrm{nm}}{\mathrm{mV}}\right]$
1	41.9	363	42.8	8.00	101	556	117	3.30	36.4	376	30.4	4.95
2	235	614	1.28 k	0.66	609	850	4.4 k	0.75	112	364	315	2.82
3	645	400	10.1 k	−0.30	1548	904	–	−0.01	345	187	3.57 k	0.19

(a) Experiment

	Rectangular				Triangular				Stepped			
Mode	f_i [kHz]	Q_i	k_i $\left[\frac{\mathrm{N}}{\mathrm{m}}\right]$	α_i $\left[\frac{\mathrm{nm}}{\mathrm{mV}}\right]$	f_i	Q_i [kHz]	k_i $\left[\frac{\mathrm{N}}{\mathrm{m}}\right]$	α_i $\left[\frac{\mathrm{nm}}{\mathrm{mV}}\right]$	f_i [kHz]	Q_i	k_i $\left[\frac{\mathrm{N}}{\mathrm{m}}\right]$	α_i $\left[\frac{\mathrm{nm}}{\mathrm{mV}}\right]$
1	35.5	–	42.8	9.30	91.6	–	132	4.9	37.8	–	32.0	7.48
2	209.8	–	1.02 k	1.86	558	–	3.30 k	1.26	116	–	217	3.60
3	572	–	12.1 k	−0.56	1434	–	48.5 k	−0.02	354	–	2.35 k	0.32

(b) FEA

excited cantilever is unsuitable for system identification due to the numerous additional dynamics unrelated to the cantilever.

45.2.3 Thermal Stiffness Calibration

The thermal noise method is particularly useful for the calibration of the dynamic spring constants of multiple eigenmodes even for arbitrary geometries [11]. It is based on measuring the cantilever vibrations due to Brownian motion caused by thermal noise. In this case, the potential energy of the harmonic oscillator is equal to the thermal energy $\frac{1}{2}k_B T = \frac{1}{2}k_i \bar{x}_i^2$ where k_B denotes the Boltzmann constant, T the equilibrium temperature, k_i the spring constant, and $\bar{x}_i^2$ the mean squared displacement of the i-th mode.

Experimentally, this is performed by measuring the velocity power spectrum at the end of the cantilever using LDV with the piezoelectric layers grounded and integrating the area underneath the resonance peak. This can be done by performing a Lorentzian function fit of the form for each mode [11]

$$S_i(f) = \frac{A_i f_i^4}{Q_i^2 (f^2 - f_i^2)^2 + f^2 f_i^2} + A_0, \tag{45.2}$$

where A_i is a fitting parameter and A_0 is the white background noise. From the fit, the mean squared velocity can be extracted as

$$\bar{v_i}^2 = \frac{\pi f_i A_i}{2 Q_i} \tag{45.3}$$

which allows to calculate the spring constant as

$$k_i = (2\pi f_i)^2 \frac{k_B T}{\bar{v}_i^2}. \tag{45.4}$$

The results are shown in Fig. 45.4. The spectra are obtained by recording the thermal vibrations in the time domain and obtaining the power spectrum density estimates using Welch's method with 64 averages, no overlap, and using the Hanning window. It can be seen how the maximum power in each resonance mode decreases with increasing mode number, leading to increasing stiffnesses in the higher eigenmodes.

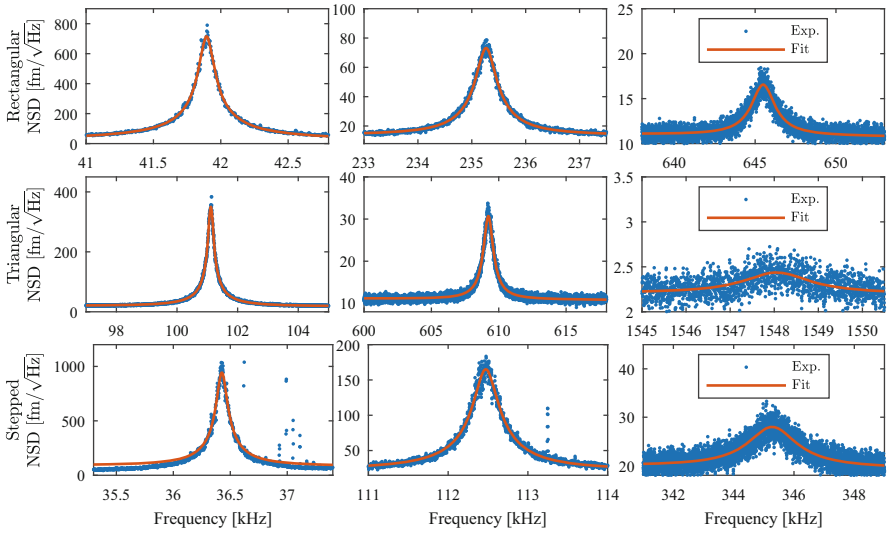

Fig. 45.4 Thermal noise spectra of the first three eigenmodes of the cantilevers

45.3 Conclusion

The results of the experimental characterization of all three cantilevers are stated in Table 45.1 together with the values obtained from a finite element analysis (FEA) using ANSYS Workbench 19.2 and CoventorWare 10.3. For details of the finite element models of piezoelectric cantilevers, the reader is referred to [12]. While the simulation tools allow for the direct extraction of the resonance frequencies and sensitivities, the dynamic stiffnesses are calculated using customized code by equating potential and kinetic energy. It can be noted that the triangular cantilever achieves the highest Q factors across all higher eigenmodes as well as the farthest spacing between resonance frequencies. The stepped rectangular cantilever has the closest spaced higher eigenmodes with lower Q factors, an enhanced second eigenmode sensitivity [6] as well as significantly reduced higher eigenmode stiffnesses. In general, the experimental values agree with the ones obtained from FEA under acceptable tolerances. Note that a full three-dimensional numerical analysis of air damping, as the biggest contributor to the Q factor, is computationally very expensive and time-consuming [13]. Therefore, it is common practice to estimate the Q factors from experimental data.

References

1. Bhushan, B.: Scanning Probe Microscopy in Nanoscience and Nanotechnology. Springer, Berlin/Heidelberg (2010)
2. Binnig, G., Quate, C.F., Gerber, C.: Atomic force microscope. Phys. Rev. Lett. **56**, 930–933 (1986)
3. Ruppert, M.G., Moheimani, S.O.R.: High-bandwidth multimode self-sensing in bimodal atomic force microscopy. Beilstein J. Nanotechnol. **7**, 284–295 (2016)
4. Rangelow, I.W., et al.: Review article: active scanning probes: a versatile toolkit for fast imaging and emerging nanofabrication. J. Vac. Sci. Technol. B **35**(6), 06G101 (2017)
5. Ruppert, M.G., Fowler, A.G., Maroufi, M., Moheimani, S.O.R.: On-chip dynamic mode atomic force microscopy: a silicon-on-insulator MEMS approach. IEEE J. Microelectromech. Syst. **26**(1), 215–225 (2017)
6. Ruppert, M.G., et al.: Multimodal atomic force microscopy with optimized higher eigenmode sensitivity using on-chip piezoelectric actuation and sensing. Nanotechnology **30**(8), 085503 (2019)
7. Rothberg, S., et al.: An international review of laser doppler vibrometry: making light work of vibration measurement. Opt. Lasers Eng. **99**, 11–22 (2017)
8. Moore, S.I., Ruppert, M.G., Yong, Y.K.: Multimodal cantilevers with novel piezoelectric layer topology for sensitivity enhancement. Beilstein J. Nanotechnol. **8**, 358–371 (2017)
9. Ruppert, M.G., Moheimani, S.O.R.: Multimode Q control in tapping-mode AFM: enabling imaging on higher flexural eigenmodes. IEEE Trans. Control Syst. Technol. **24**(4), 1149–1159 (2016)
10. Ruppert, M.G., Yong, Y.K.: Note: guaranteed collocated multimode control of an atomic force microscope cantilever using on-chip piezoelectric actuation and sensing. Rev. Sci. Instrum. **88**(8), 086109 (2017)
11. Sader, J.E., et al.: Spring constant calibration of atomic force microscope cantilevers of arbitrary shape. Rev. Sci. Instrum. **83**(10), 103705 (2012)
12. Moore, S.I., Ruppert, M.G., Yong, Y.K.: An optimization framework for the design of piezoelectric AFM cantilevers. Precis. Eng. **60**, 130–142 (2019)
13. Kaajakari, V.: Practical MEMS. Small Gear Publishing, Las Vegas (2009)